Magnetic connectivity in the time-dependent corona and heliosphere

Lionello, R. ORCID: https://orcid.org/0000-0001-9231-045X, Downs, C. ORCID: https://orcid.org/0000-0003-1759-4354, Mason, E. I. ORCID: https://orcid.org/0000-0002-8767-7182, Linker, J. A. ORCID: https://orcid.org/0000-0003-1662-3328, Riley, P. ORCID: https://orcid.org/0000-0002-1859-456X and Owens, M. J. ORCID: https://orcid.org/0000-0003-2061-2453
(2026) Magnetic connectivity in the time-dependent corona and heliosphere. The Astrophysical Journal Letters, 1001 (1). L23. ISSN 2041-8213 doi: 10.3847/2041-8213/ae5791
Available at https://centaur.reading.ac.uk/129317/

The Astrophysical Journal Letters, 1001:L23 (7pp), 2026 April 10 https://doi.org/10.3847/2041-8213/ae5791

Magnetic Connectivity in the Time-dependent Corona and Heliosphere

Roberto Lionello[1], Cooper Downs[1], Emily I. Mason[1], Jon A. Linker[1], Pete Riley[1], and Mathew J. Owens[2]
[1] Predictive Science Inc., 9990 Mesa Rim Rd., Ste. 170, San Diego, CA 92121, USA
[2] Department of Meteorology, University of Reading, Reading, UK
Received 2026 January 28; revised 2026 March 14; accepted 2026 March 22; published 2026 April 10

Abstract

Magnetic flux fills the heliosphere, expands outward from the solar corona, and is fundamentally related to the structure and dynamics of the solar corona and solar wind. Open magnetic flux and the fast wind are thought to originate from open magnetic field lines in coronal holes. Less understood processes in the streamer belt and the boundaries of coronal holes, associated with the more variable slow wind, may be formed by interchange reconnection between open and closed magnetic flux. Interchange reconnection is thought to give rise to field lines that are "folded," i.e., that turn back on themselves. The properties of strahl electrons measured in the solar wind give clues to the heliospheric magnetic connectivity. Unidirectionally outward strahl indicates open field lines, while bidirectional strahl is associated with closed magnetic flux and coronal mass ejections (CMEs). Inward-directed, unidirectional strahl is believed to indicate folded flux. We use two time-dependent, flux-evolutionary magnetohydrodynamic (MHD) models of the combined corona and heliosphere, one for a solar-minimum configuration and one for the 2024 total solar eclipse, to investigate the magnetic connectivity of the corona/heliosphere system. We examine how magnetic connectivity varies with distance from the Sun in the two configurations. We evaluate the evolutionary effects by contrasting time-dependent results with the corresponding steady-state calculations and compare the model connectivities with statistical studies of strahl. The connectivities in the time-evolving simulations are roughly consistent with observed strahl occurrence rates, while those from the steady-state models are not. Our results suggest that complex magnetic connectivities are ubiquitous in the heliosphere.

Unified Astronomy Thesaurus concepts: Solar corona (1483); Solar magnetic fields (1503); Magnetohydrodynamical simulations (1966); Solar wind (1534); Solar magnetic flux emergence (2000)

Materials only available in the online version of record: animation

1. Introduction

The solar magnetic field expands outward from the solar surface and fills the corona and the heliosphere. It plays a key role in the physics of the solar wind. Many of the outstanding questions in heliophysics revolve around understanding how the properties that are measured in situ in the solar wind were created back at the Sun. In the presence of ideal flows and in the reference frame corotating with the Sun, the solar wind plasma flow is aligned with the magnetic field. In this approximation, tracing the magnetic connectivity of plasma parcels encountered in the heliosphere back to the Sun reveals their solar origin. The magnetic field connectivity is also important for the transport and propagation of solar energetic particles (SEPs), which are guided along magnetic field lines from their generation near the Sun to locations in the heliosphere.

In terms of solar connectivity, magnetic field lines can either be open (one end connected with the photosphere), closed (both ends connected with the photosphere), or disconnected (neither end connected with the photosphere). In the standard paradigm of coronal structure (e.g., D. H. Mackay & A. R. Yeates 2012; E. Priest 2014; J. A. Linker et al. 2017), the open field originates primarily in coronal holes (CHs), which are defined as low-intensity emission regions in the EUV and in X-rays (J. D. Bohlin 1977; J. B. Zirker 1977), while magnetically closed field regions form the streamer belt. From the low coronal perspective, open field lines are simply those that stretch far enough away from the Sun that they are carried out by the solar wind and no longer confine the plasma near the Sun. This definition is ambiguous from the heliospheric perspective, as these different connectivities may be present in the field encountered by in situ spacecraft. The properties of the field in the heliosphere appear to be associated with the origin of the solar wind, where fast wind is found to emanate from deep within CHs and expected to be "open" in the heliosphere. The slow wind is associated with the streamer belt and the boundaries of CHs (L. Abbo et al. 2016). L. A. Fisk et al. (1998) argued that the so-called interchange reconnection between closed and open magnetic flux releases the plasma that forms the slow solar wind. The topological properties associated with this process are elucidated in the S-web model (S. K. Antiochos et al. 2011; J. A. Linker et al. 2011; V. S. Titov et al. 2011). Interchange reconnection within the S-web is also expected to create magnetic fields that are locally inverted or turned back on themselves (N. U. Crooker et al. 2004), which we refer to here as "folded" flux. Folded flux could also be generated by shear in adjacent solar wind flux tubes that causes the folds to develop over time in the heliosphere as argued by M. J. Owens et al. (2018). Such shear patterns could also result from interchange reconnection, and measurements of B_r (M. Lockwood et al. 2009) and of strahl at a range of heliocentric distances (A. R. Macneil et al. 2020) support this possibility.

Table 1
Computer Simulations Considered in This Work

Label	Coronal Resolution	Heliospheric Resolution	Outer Boundary ($R_\odot$)	Conditions	Flux Evolution	References for Coronal Run
SMTD	269 × 181 × 361	763 × 181 × 361	430	Solar Minimum	719 hr	R. Lionello et al. (2023)
SMSS	269 × 181 × 361	401 × 181 × 361	230	Solar Minimum	No	E. I. Mason et al. (2023)
E24TD	284 × 292 × 630	1598 × 334 × 720	430	Eclipse 2024	775 hr	C. Downs et al. (2025)
E24SS	284 × 292 × 630	801 × 334 × 720	230	Eclipse 2024	No	C. Downs et al. (2025)

While the true connectivity of the magnetic field lines cannot be directly measured in situ, the properties of electrons propagating in the solar wind can provide important clues about their connectivity and geometry. Results from the HELIOS plasma experiment showed that electrons usually exhibit a suprathermal tail known as strahl (H. Rosenbauer et al. 1977). When a strahl is observed, it is often in one direction, i.e., going outward from the Sun either parallel or antiparallel to the heliospheric magnetic field. However, counterstreaming strahl are also present, which may be evidence of closed magnetic field lines or, as J. T. Gosling et al. (1987) argued, magnetic flux connected with coronal mass ejections (CMEs). B. R. Anderson et al. (2012) presented a statistical survey of strahl using measurements from 1998 to 2002 and found that a strahl is present $\geqslant$75% of the time, with a unidirectional strahl present 65% of the time, and a 10% occurrence rate for counterstreaming electrons. M. J. Owens et al. (2017) noted the occurrence of unidirectional, sunward-directed strahl as an indication of folded magnetic flux and emphasized its importance for estimating the open magnetic flux in the heliosphere, which can be overestimated if simple averaging of the interplanetary unsigned flux is employed (M. J. Owens et al. 2008). M. J. Owens et al. (2017) provided estimates of the occurrence rates of all four strahl: unipolar outward (∼69%), bidirectional (∼4%), inverted (∼17%), and absent (∼10%). A. M. Frost et al. (2022) expanded upon the M. J. Owens et al. (2017) study to look at statistics over 27 yr, finding similar occurrence rates, although notably more bidirectional strahl (∼11%). These differences result from thresholds used to define the presence of strahl at 0° and 180°.

In this work, we explore how magnetic connectivity varies temporally and spatially in the solar corona and heliosphere and find that this is an essentially dynamic process. To show this, we use time-dependent (TD), flux-evolutionary simulations of the corona (R. Lionello et al. 2023; C. Downs et al. 2025) and heliosphere, with the heliospheric evolution coupled to the corona using the method of R. Lionello et al. (2013). To understand the importance of flux evolution, TD results are compared with the correspondent SS cases (E. I. Mason et al. 2023). Two different configurations are considered here: a solar minimum case (as in R. Lionello et al. 2023) and the time around the 2024 total solar eclipse, near solar maximum (C. Downs et al. 2025). For each configuration, we calculate the magnetic connectivity as a function of the distance from the solar surface and determine what fractions of open, closed, and disconnected flux are present at 1 au. We compare the model results with strahl occurrence rates from the B. R. Anderson et al. (2012), M. J. Owens et al. (2017), and A. M. Frost et al. (2022) studies.

In Section 2, we describe the combined models and the computations; in Section 3, we show and compare connectivity in the models. In the last section, we discuss the physical implications of our results.

2. The Combined, Time-dependent Magnetohydrodynamic Models

Our calculations have been obtained with the Magnetohydrodynamic Algorithm outside a Sphere (MAS) magnetohydrodynamic (MHD) model, which has been used for modeling both the solar corona and the heliosphere (most recently and respectively, C. Downs et al. 2025; P. Riley et al. 2025).

2.1. The Coronal Model

The coronal model (see Z. Mikić et al. 2018 and R. Lionello et al. 2023 for a full description) is a 3D, resistive, thermodynamic MHD rendition of the solar corona spanning from the solar surface to 30 $R_\odot$. Wave-turbulence-driven (WTD) heating and acceleration are prescribed (R. Lionello et al. 2014; C. Downs et al. 2016; Z. Mikić et al. 2018). Although we have always advanced MAS equations in time, in the past, we used to look for a steady state (SS). Now we also follow the TD evolution of the corona by incorporating surface flux evolution at the photospheric boundary to drive the system. This is done by prescribing at the inner boundary, $r = R_\odot$, a sequence of magnetic flux maps as well as differential rotation and meridional flows (R. Lionello et al. 2023). Energization of the magnetic field can also be introduced to obtain more realistic structures and better match the observed corona (C. Downs et al. 2025).

2.2. The Heliospheric Model

From a shell at $r = 25\,R_\odot$ (i.e., where the flow is already supersonic and super-Alfvénic) within the coronal model, we extract a time sequence of fields (magnetic, velocity, density, and temperature). These are prescribed as boundary conditions at the lower boundary of the heliospheric model to drive its evolution (R. Lionello et al. 2013). The outer boundary is set at $r = 230$ for SS runs, or $430\,R_\odot$ for evolutionary runs, a further extension being necessary to minimize boundary effects at 1 au. The heliospheric model employs the so-called polytropic approximation (J. A. Linker et al. 2003), which uses a simple adiabatic energy equation, and, in the present case, the ratio of specific heats is $\gamma = 3/2$.

2.3. Simulations

We performed four simulations using the coupled coronal and heliospheric models. These are summarized in Table 1. The coronal part of the SMTD simulation is described in R. Lionello et al. (2023). The TD evolution of the corona is calculated for 719 hr, in response to surface magnetic field

maps and flows corresponding to a solar minimum (SM) configuration obtained from the model of C. J. Schrijver & M. L. DeRosa (2003). The initial condition for the heliosphere is a potential field extrapolation of the coronal magnetic flux at 25 $R_\odot$. The same radial velocity and temperature from the said surface are prescribed for each internal point of the same latitude and longitude, while the density is scaled with r^{-2} (R. Lionello et al. 2013). The coronal sequence is then used to drive the heliosphere. Since the signal from the driving propagates from the lower boundary at 25 $R_\odot$ outward, it takes ≈100 hr for it to reach Earth. During this relaxation time, conditions at 1 au only feel the effect of rotation.

For the SMSS simulation, we use one of the coronal SS solutions presented in E. I. Mason et al. (2023). It was obtained by using the surface flux distribution from the corresponding TD model at 526 hr as a static boundary condition and relaxing for about 80 hr. Then, the conditions at 25 $R_\odot$ from this relaxed state are propagated outward into the heliosphere for about 240 hr to obtain an SS throughout.

The E24TD simulation is based on the prediction of the 2024 total solar eclipse (E24) as described in C. Downs et al. (2025). For 775 hr, photospheric magnetic field observations were updated, processed, and assimilated as boundary conditions at $r = R_\odot$ in near real time (R. M. Caplan et al. 2025). Energizing TD electric fields were also applied at the boundary (Z. Mikić et al. 2018). The coronal calculation is then used to obtain a TD solution for the heliosphere. The initialization of the heliosphere is specified as in the SMTD case. Then, the values at 25 $R_\odot$ extracted from the coronal calculation are used to drive the heliosphere for 775 hr. Finally, similar to the SMSS case, the E24SS simulation is obtained from one of the SS calculations studied in C. Downs et al. (2025), who fixed the surface flux distribution at 320 hr and relaxed the corona for 80 hr. This solution is then propagated outward with the heliospheric MAS for 240 hr to obtain an overall SS.

3. Connectivity

We now examine the connectivity by tracing field lines in either direction from points within the combined coronal and heliospheric domain. Closed regions have both endpoints at $r = R_\odot$, open regions have one point at $r = R_\odot$ and one at the outer boundary, and disconnected regions have both endpoints at the outer boundary. For the TD runs, we trace field lines at times well after the initial transient phase (≈200 hr), during which the signal of the first time sequence travels from the 25 $R_\odot$ shell to reach the outer boundary at 2 au. Figure 1 shows the area fractions of spherical surfaces as a function of radius. The open field fractions are in orange, the closed field in green, and the disconnected in sky blue. The TD quantities are traced with continuous lines, the SS with dotted lines. Panel (a) is for the SM cases; panel (b) is for the E24 cases. As one moves outward, the area of open magnetic flux (orange) increases rapidly to fill the corona and then asymptotically tends to a plateau. However, while SMTD and SMSS have similar open-area percentages, E24TD has distinctively less open areas than E24SS. Unsurprisingly, the area of closed magnetic flux (green) decreases rapidly in the first few solar radii from the solar surface. SS runs have more open areas than TD runs. This is particularly true for E24TD in comparison with E24SS.

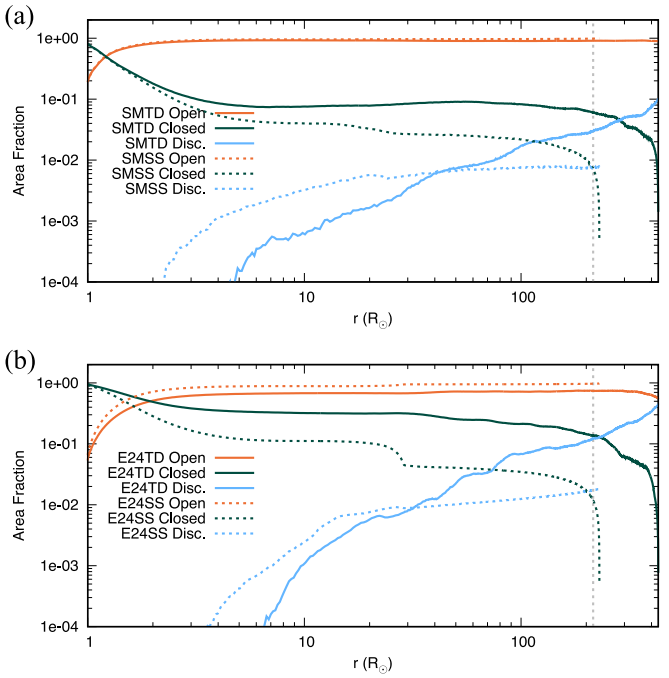

Figure 1. Area fractions of the spherical surface at different radii occupied by magnetic field lines of different connectivity: (a) SM runs; (b) E24 runs. The dotted vertical line is 1 au.

The area fraction of disconnected flux (sky blue) remains negligible for the SS simulations ($\lesssim$1%) but generally grows with increasing distance in the TD simulations. This difference is related to the inherent dynamical evolution present in the TD simulations, in which the heliospheric current sheet (HCS) periodically reconnects and ejects material and magnetic flux ropes (e.g., V. Réville et al. 2020). This process brings together the flux immediately adjacent to the HCS, which is generally closed initially but eventually involves open flux on either side. When two open flux tubes on either side reconnect, this forms disconnected flux that maps from the location of the flux rope as it propagates to the outer boundary. The superposition of several of these structures in height all advecting outward as they leave the domain leads to the relative increase of disconnected flux with height. The relative amount of closed and disconnected flux is also increased in the E24TD simulation by the energization scheme incorporated into the boundary driving, which leads to the formation of several flux ropes and small eruptions originating from the low corona.

Nearing the outer boundary of the TD simulations, we see a drop in the closed flux and a rise in the disconnected flux. Because the simulation must include an outer boundary, its presence introduces the potential for miscounting closed flux within flux ropes as disconnected as the structure nears the outer boundary. This is primarily our motivation for placing outer boundary of the heliospheric simulation at 2 au while focusing on flux fractions at 1 au.

In Figure 2, we present maps of the connectivity of the runs of Table 1 on Mercator projections at 1 au ((a), (c), (e), and (g)) and in a cut at longitude = 0° ((b), (d), (f), and (h)). We distinguish between open flux of positive (maroon) and negative (navy) polarity. Sky blue is used for disconnected flux and green for closed flux; the white dashed line indicates where $B_r = 0$, which for SS runs marks the HCS. In agreement

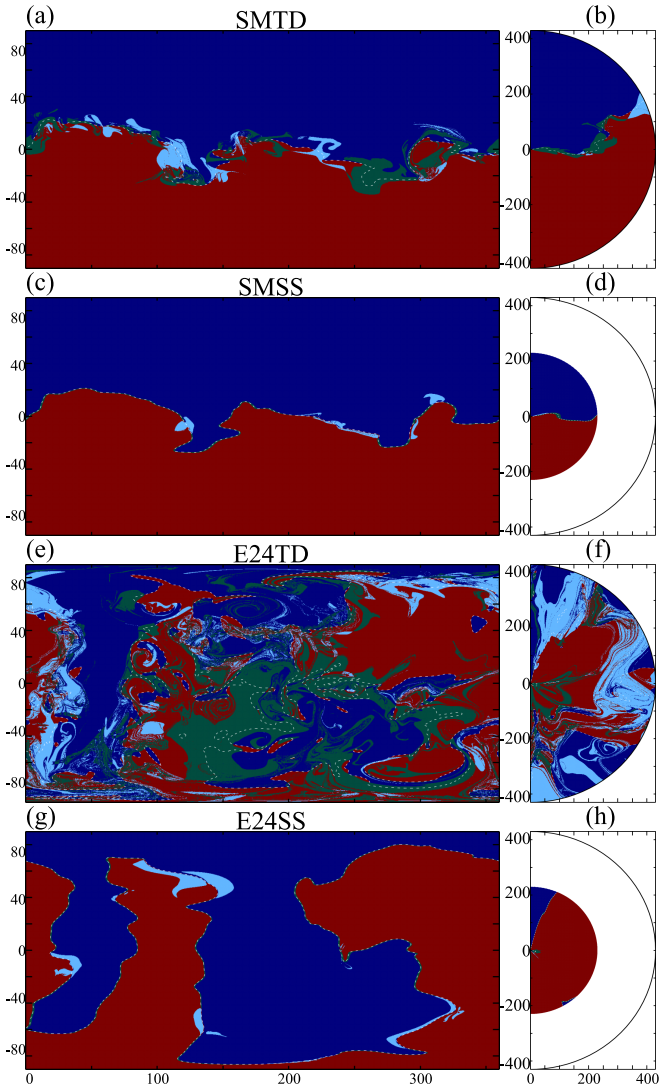

Figure 2. Connectivity maps for the runs of Table 1. Color codes: navy, open negative flux; maroon, open positive flux; green, closed flux; sky blue, disconnected flux; and white dashed line, $B_r = 0$. (a) Mercator projection at 1 au for SMTD; (b) cut at 0° longitude for SMTD. (c) Same as (a) for SMSS. (d) Same as (b) for SMSS. (e), (f) Same as (a) and (b), respectively, for E24TD. (g), (h) Same as (c) and (d), respectively, for E24SS.

with Figure 1, the TD runs show far wider areas of disconnected flux compared with SS runs. This is especially true for E24TD ((e) and (f)), when compared with E24SS ((g) and (h)). Areas of closed flux are also more extended in the TD runs. The boundaries between the different areas are more complex in TD runs than in SS runs. This is especially evident if one compares panel (e) with (g) (E24TD versus E24SS).

We now turn our attention to the temporal evolution of connectivity in the ±6° latitude zone at 1 au. This roughly corresponds to the extension of the solar B angle (the heliographic latitude of the central point of the solar disk), within which the Earth and most spacecraft orbit. The results are displayed in Figure 3. For each of the simulations of Table 1, we show the area fractions of the zone corresponding to each connectivity, i. We distinguish between folded and not-folded open field lines: a point of an open field line is considered folded if it belongs to the sunward portion of the said line. Each area fraction a_i corresponding to each

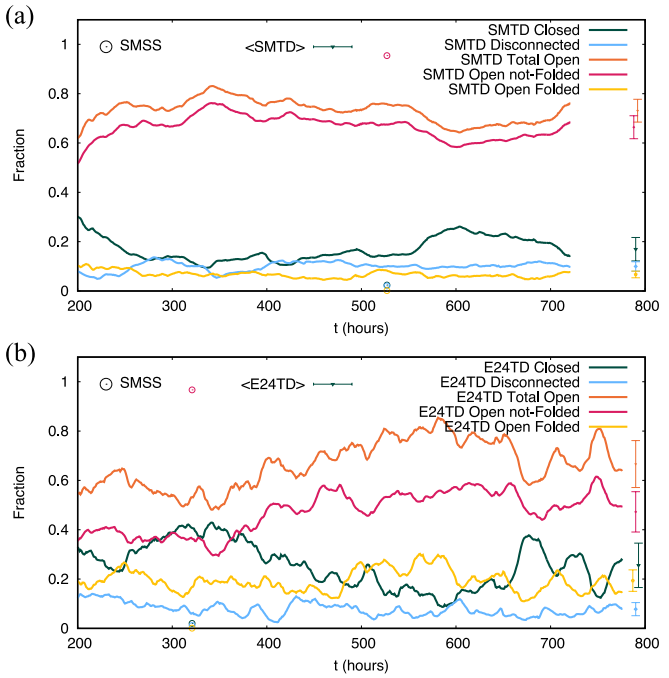

Figure 3. Connectivity fractions as a function of time in the ±6° latitude zone: (a) SM runs; (b) E24 runs. We have removed the first 200 hr of the simulations, during which the heliospheric relaxation phase occurs. Closed flux is green, disconnected is sky blue, open folded flux is gold, open not-folded is rose, and total open flux is orange. Average values with standard deviation errors from 200 hr to the end of the TD simulations are shown on the right within each plot. The values for the SS simulations are shown as circles at 526 hr for SMSS and 320 hr for E24SS.

connectivity i (closed, disconnected, open folded, and open not-folded) is defined as follows:

$$a_i = \frac{1}{a}\int_0^{\pi}\int_0^{2\pi} z(\theta)c_i(\theta,\,\phi)\sin\theta\; d\theta\; d\phi,$$
$$a = \int_0^{\pi}\int_0^{2\pi} z(\theta)\sin\theta\; d\theta\; d\phi, \qquad (1)$$

where $z(\theta)$ is 1 in the ±6° equatorial zone and 0 elsewhere, and $c_i(\theta, \phi)$ is 1 where the connectivity is i and 0 elsewhere. While the TD simulations have evolving values in time (lines), the SSs have constant fractions (circles) calculated at the end of the relaxation phase. All the flux-fraction lines of SMTD show lower variability than those of E24TD. This can be appreciated by examining the right section of Table 2, which shows the average and standard deviation for each connectivity of the TD runs in the interval between 200 hr (i.e., after the transient phase) and the end of the simulation. If we compare TD with SS runs, we find that SS runs are dominated by open not-folded flux, while TD runs have significant fractions of all connectivities.

To better illustrate the properties of the simulation, we have flown the trajectory of the Earth in E24TD from 200 hr to the end of the calculation. We have calculated the magnetic field lines along the trajectory and colored them with the same color scheme of Figure 3, except that we do not mark the sign of the magnetic flux. The result is displayed in Figure 4, which has a 3D rendering of the orbit on top and a Mercator projection in the bottom. The initial point is marked with a blue arrow.

Table 2
The Strahl Statistics of B. R. Anderson et al. (2012, A12), M. J. Owens et al. (2017, O17), and A. M. Frost et al. (2022, F22) Compared with the Connectivities of Figure 3

Strahl	A12	O17	F22	SMTD	SMSS	E24TD	E24SS	Connectivity
Unidirectional	$\geqslant$65	85.7	80.5	73 ± 5	96	66 ± 10	97	Total Open
↪ Antisunward	⋯	68.7	65.5	66 ± 5	96	47 ± 8	97	↪ Open Not Folded
↪ Sunward	⋯	17.0	15.0	7 ± 1	0	19 ± 4	0	↪ Open Folded
Counterstreaming	≈10	4.1	11.3	17 ± 5	2	26 ± 9	1	Closed
Unclassified/Absent	$\leqslant$25	10.1	8.3	10 ± 2	2	8 ± 3	2	Disconnected

"↪" Indicates unidirectional strahl.

4. Discussion and Conclusion

We have examined the magnetic connectivity in the corona and heliosphere in four MHD simulations, covering the possible combinations between flux evolution versus SS and solar minimum versus maximum. As we move outward from the Sun, the fraction of disconnected flux and folded flux in TD runs grows much faster than in SS. This can be interpreted as an effect of the photospheric driving that continuously stresses the corona, leading to reconnection in the HCS and small CMEs. The decrease in closed flux areas is somewhat slower in TD runs (especially for E24TD) than in SS. These trends lead to dramatically different pictures at 1 au, where for SS runs, we simply find two areas of open flux of opposite polarity separated by the HCS, while in TD simulations, intertwined areas of disconnected and closed flux are disseminated along the $B_r = 0$ curve (or curves) of the HCS. We have then focused our attention on the zone at 1 au where Earth and most spacecraft orbit and found quantitative evidence that the connectivity frequencies of closed, disconnected, and (to a lesser degree) open flux between TD and SS runs are incompatible.

The connectivity of magnetic field lines appears to be related to the propagation of electrons and, in particular, with their suprathermal tail, or strahl. The statistics of long-term studies of strahl observations at 1 au from the ACE/WIND spacecraft are provided in the right section of Table 2 and can be summarized as follows: The survey of B. R. Anderson et al. (2012, hereafter A12) for the 1998–2002 time period (increasing phase toward maximum) concludes that strahl occurred $\geqslant$75% of the time, while counterstreaming occurred strahl about 10% of the time. We deduce that unidirectional strahl was observed for $\geqslant$65% of the interval and no strahl for $\leqslant$25%. In the statistics provided by M. J. Owens et al. (2017, hereafter O17) and A. M. Frost et al. (2022, hereafter F22) a further distinction is introduced besides undetermined and counterstreaming strahl: unidirectional strahl can either be directed away from or toward the Sun. This inverse strahl is associated with a switchback or folding of the magnetic field.

Comparing the observed strahl statistics (Table 2, left) to the average connectivity fractions of our simulations (Table 2, right), we find that the TD and SS simulations contrast quite differently with the observations. Regarding the total open magnetic flux, the SS simulations, by virtue of being almost entirely open ($\geqslant$96%), largely overpredict the measured frequency of unidirectional strahl. Conversely, the TD simulations underpredict the average frequencies determined from the long-term O17 and F22 surveys but are compatible with the A12 survey, which covers a slightly more active than average period during the ascending phase of solar cycle 23.

Splitting the strahl and open flux statistics into the antisunward (open not-folded) and the sunward categories (open and folded), we find that the SS simulations are wholly incompatible with the relative frequency of folded flux (0% versus 15%–17%), which is not surprising because such structures cannot typically be produced in an SS configuration. The TD simulations, on the other hand, average between 7% and 19% folded flux, respectively, similar to the observational determinations from the O17 and F22 surveys. This underscores the importance of TD dynamics in forming the folded magnetic structures encountered in the heliosphere at 1 au.

A similar picture emerges when comparing the counterstreaming (closed) and unclassified/absent (disconnected) categories to the SS and TD simulations. The SS simulations produce very little of either closed or disconnected flux while the TD simulations create a healthy amount, of order ∼20% and ∼10%, for each respective category. As with the folded open flux category, the relative fractions from the TD simulations appear much more compatible with the observational studies than the SS simulations, again implying that the SS simulations are missing an essential ingredient to forming these magnetic structures.

That said, caution must be exercised when explicitly ascribing observed strahl signatures to different connectivity categories of traced magnetic field lines. As discussed in A12, electron scattering processes during transit along magnetic field lines can influence the relative width and amplitude of the suprathermal electron population. The importance of scattering is highly correlated with the overall field line length (fade-out) as well as the local plasma properties encountered, both of which can vary significantly between "simple" spiral flux tubes in the heliosphere and the folded or twisted magnetic field lines within the HCS or ICMEs (Figure 4). Additionally, the observational criteria used to delineate different connectivity categories based on strahl is not uniform between studies and have led to variation in the measured statistics.

For example, comparing the relative frequency of closed flux in the TD simulations (∼20%) to the counterstreaming frequency observational surveys (4%–11%), it appears that the TD simulations overestimate the relative amount of closed magnetic flux that is observed in the heliosphere. While this is certainly possible given the fidelity of our current data-driven simulation capabilities, closed field lines are identified by an instantaneous field line trace through the model, while time of flight and scattering processes dictate the observationally measured suprathermal signal. For closed field lines with an apex well beyond 1 au, it is almost guaranteed that one coronal footpoint will have a much shorter path length to the in situ measurement point than the other footpoint, and the relative length differences can be extreme for long or highly twisted (or folded) field lines. In this

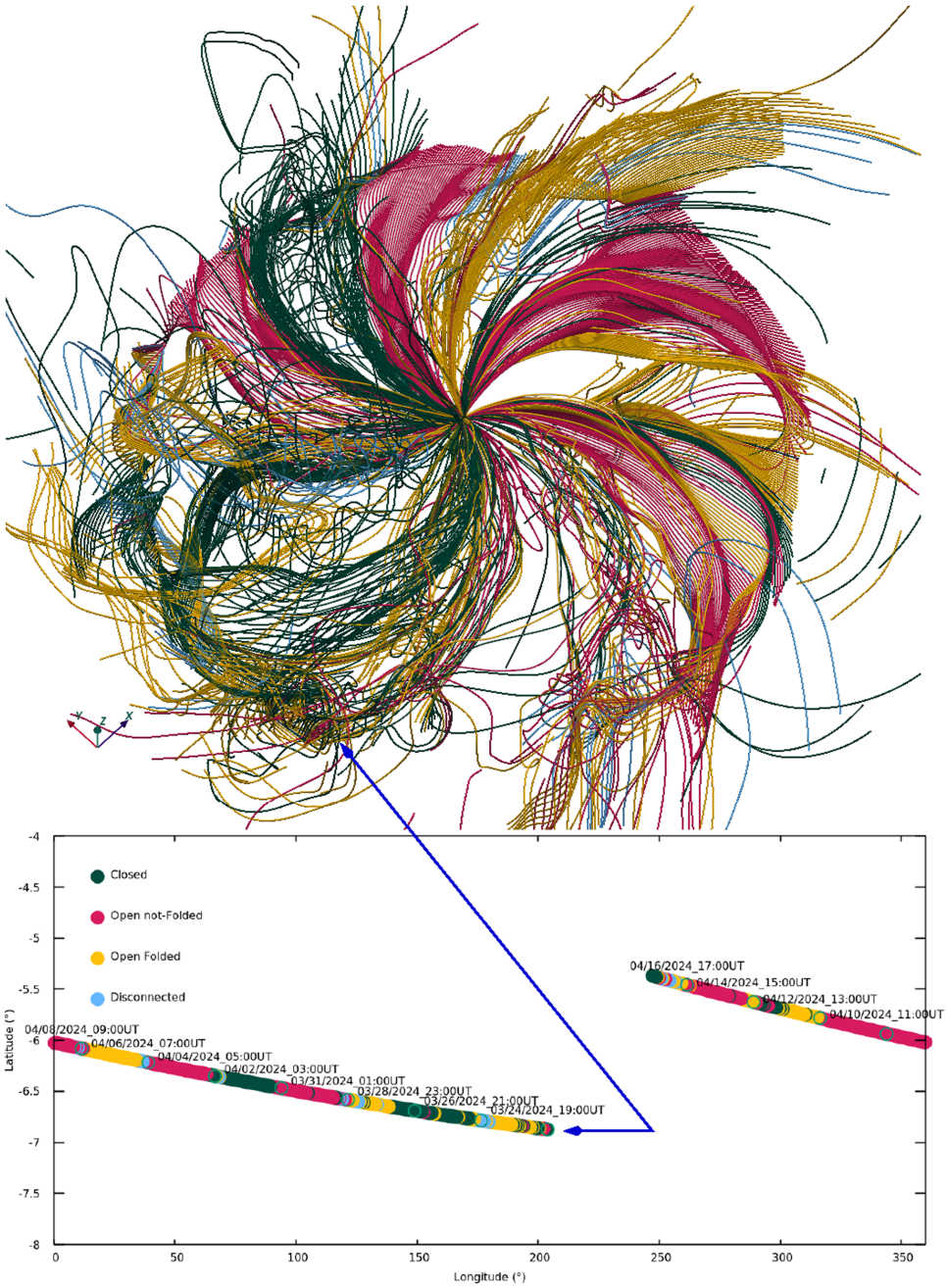

Figure 4. Field line connectivity along the trajectory of Earth in the E24TD calculation, from 2024 March 24 at 19:00 UT (200 hr in the simulation) to the end (2024 April 16 17:00 UT). Top: 3D rendering. An animation showing all angles is available. Bottom: the trajectory in the longitude-latitude plane. As in Figure 3, closed field lines are green, open not-folded are rose, open and folded are gold, and disconnected are sky blue. The double blue arrow shows the beginning of the trajectory. (An animation of this figure is available in the online article.)

sense, one could argue that the measured counterstreaming frequencies are a lower limit on the overall amount of closed flux in the heliosphere. On the other hand, the extent to which this loss would take place within the 2 au TD model domain is debatable and depends strongly on field line length, curvature, and transport processes and needs to be studied further.

Overall, our investigation illustrates the importance of including magnetic flux evolution at the solar surface when investigating magnetic connectivity of the corona and heliosphere. In future studies, we aim to use this TD modeling paradigm to explore other ways in which combined coronal and heliospheric TD and SS systems inherently differ. This may be especially important for capturing the instantaneous connectivity during SEP events and for identifying solar source regions with ballistic mapping techniques.

The concept of a background SS corona and heliosphere can be an incredibly useful construct to understand the physics of solar wind heliospheric structure (e.g., the canonical Parker spiral and ballerina skirt HCS). However, ultimately, it is the inherent dynamics of the system—as driven by photospheric flux evolution and associated coronal dynamics—that continually perturb and disrupt this background. Such dynamics can only be captured by truly data-driven MHD modeling, and the relatively good agreement of the TD simulations with strahl statistics and comparatively poor agreement of the SS simulations underscores this point.

Acknowledgments

We thank the NASA High-End Computing (HEC) Program through the NASA Advanced Supercomputing Division (NAS) at Ames Research Center for allocations on the Pleiades, Electra, and Aitken supercomputers and the NSF ACCESS program for allocations on the Expanse supercomputer at the San Diego Supercomputer Center (SDSC), which were used to run the simulations. These simulations would not have been possible without the generous support from personnel at both centers, as well as the use of special priority queues. This work was supported by the NASA Living With a Star Strategic Capabilities program (80NSSC22K0893), NSF SHINE program (AGS 2501333), NASA Living With a Star Science program (80NSSC20K0192 and 80NSSC22K1021), and NSF PREEVENTS program (ICER 1854790). We thank Dr. Susan T. Lepri for a private conversation about strahl measurements.

ORCID iDs

Roberto Lionello https://orcid.org/0000-0001-9231-045X
Cooper Downs https://orcid.org/0000-0003-1759-4354
Emily I. Mason https://orcid.org/0000-0002-8767-7182
Jon A. Linker https://orcid.org/0000-0003-1662-3328
Pete Riley https://orcid.org/0000-0002-1859-456X
Mathew J. Owens https://orcid.org/0000-0003-2061-2453

References

Abbo, L., Ofman, L., Antiochos, S. K., et al. 2016, SSRv, 201, 55
Anderson, B. R., Skoug, R. M., Steinberg, J. T., & McComas, D. J. 2012, JGRA, 117, A04107
Antiochos, S. K., Mikić, Z., Titov, V. S., Lionello, R., & Linker, J. A. 2011, ApJ, 731, 112
Bohlin, J. D. 1977, in Coronal Holes and High Speed Wind Streams, ed. J. B. Zirker (Colorado Associated Univ. Press), 27
Caplan, R. M., Stulajter, M. M., Linker, J. A., et al. 2025, ApJS, 278, 24
Crooker, N. U., Kahler, S. W., Larson, D. E., & Lin, R. P. 2004, JGRA, 109, A03108
Downs, C., Linker, J. A., Caplan, R. M., et al. 2025, Sci, 388, 1306
Downs, C., Lionello, R., Mikić, Z., Linker, J. A., & Velli, M. 2016, ApJ, 832, 180
Fisk, L. A., Schwadron, N. A., & Zurbuchen, T. H. 1998, SSRv, 86, 51
Frost, A. M., Owens, M., Macneil, A., & Lockwood, M. 2022, SoPh, 297, 82
Gosling, J. T., Baker, D. N., Bame, S. J., et al. 1987, JGR, 92, 8519
Linker, J. A., Caplan, R. M., Downs, C., et al. 2017, ApJ, 848, 70
Linker, J. A., Lionello, R., Mikić, Z., Titov, V. S., & Antiochos, S. K. 2011, ApJ, 731, 110
Linker, J. A., Mikić, Z., Lionello, R., et al. 2003, PhPl, 10, 1971
Lionello, R., Downs, C., Linker, J. A., et al. 2013, ApJ, 777, 76
Lionello, R., Downs, C., Mason, E. I., et al. 2023, ApJ, 959, 77
Lionello, R., Velli, M., Downs, C., et al. 2014, ApJ, 784, 120
Lockwood, M., Owens, M., & Rouillard, A. P. 2009, JGRA, 114, A11104
Mackay, D. H., & Yeates, A. R. 2012, LRSP, 9, 6
Macneil, A. R., Owens, M. J., Wicks, R. T., et al. 2020, MNRAS, 494, 3642
Mason, E. I., Lionello, R., Downs, C., et al. 2023, ApJL, 959, L4
Mikić, Z., Downs, C., Linker, J. A., et al. 2018, NatAs, 2, 913
Owens, M. J., Arge, C. N., Crooker, N. U., Schwadron, N. A., & Horbury, T. S. 2008, JGRA, 113, A12103
Owens, M. J., Lockwood, M., Barnard, L. A., & MacNeil, A. R. 2018, ApJL, 868, L14
Owens, M. J., Lockwood, M., Riley, P., & Linker, J. 2017, JGRA, 122, 10,980
Priest, E. 2014, Magnetohydrodynamics of the Sun (Cambridge Univ. Press)
Réville, V., Velli, M., Rouillard, A. P., et al. 2020, ApJL, 895, L20
Riley, P., Lionello, R., & Rivera, Y. J. 2025, ApJ, 979, 204
Rosenbauer, H., Schwenn, R., Marsch, E., et al. 1977, JGZG, 42, 561
Schrijver, C. J., & DeRosa, M. L. 2003, SoPh, 212, 165
Titov, V. S., Mikić, Z., Linker, J. A., Lionello, R., & Antiochos, S. K. 2011, ApJ, 731, 111
Zirker, J. B. 1977, RvGSP, 15, 257